

Scanning Electrochemical Microscopy. 12. Theory and Experiment of the Feedback Mode with Finite Heterogeneous Electron-Transfer Kinetics and Arbitrary Substrate Size

Allen J. Bard,* Michael V. Mirkin, Patrick R. Unwin,[†] and David O. Wipf

Department of Chemistry and Biochemistry, The University of Texas at Austin, Austin, Texas 78712
(Received: August 16, 1991; In Final Form: October 28, 1991)

The theory of the feedback mode of the scanning electrochemical microscope (SECM) is extended to include the cases of both finite heterogeneous electron-transfer (et) kinetics at the substrate and arbitrary substrate sizes. Theoretical treatments are developed using two independent approaches: (i) the formulation and numerical solution of multidimensional integral equations and (ii) the alternating direction implicit finite-difference method. Working curves and tabulated data are presented for both quasi-reversible and irreversible et reactions on the substrate. The range of et rate constants accessible to measurement via this technique is identified. Fast heterogeneous et rate constants, up to $1\text{--}20\text{ cm s}^{-1}$, should be measurable by SECM feedback techniques with the range of tip sizes currently employed (disks with diameters of $2\text{--}25\text{ }\mu\text{m}$). The theoretical treatments are complemented with experiments on the oxidation of $\text{Ru}(\text{NH}_3)_6^{2+}$ in aqueous solutions of pH 4.0 and of Fe^{2+} in $1\text{ M H}_2\text{SO}_4$ at glassy-carbon electrodes, as examples of quasi-reversible and irreversible systems, respectively. Simulated current-distance curves for diffusion-controlled feedback are given for a range of substrate sizes; under certain conditions, conductive features $10\text{--}20$ times smaller than the tip electrode should be identifiable by SECM. Experiments involving the oxidation of $\text{Ru}(\text{NH}_3)_6^{2+}$ at Pt ultramicrodisk electrodes of different sizes, employed as model finite substrates, agree well with the theoretical predictions for finite substrate effects in SECM.

Introduction

We describe, through theoretical models and experimental studies, how the scanning electrochemical microscope (SECM) can be used to measure heterogeneous rate constants at the solid/liquid interface. Such measurements are useful in the reactive imaging of surfaces. The SECM¹⁻¹⁰ has been used to study different types of interfaces in contact with liquids. It is usually operated in the feedback mode, where changes in the faradaic current at a small disk electrode (the tip) as a function of the distance between tip and sample (the substrate) can provide information about substrate topography and conductivity. The SECM can thus provide images, at micrometer or submicrometer resolution, of both conductors and insulators. In addition to its imaging capabilities, the SECM can also be used to measure the rates of heterogeneous processes at the substrate¹⁰ and homogeneous chemical reactions¹¹ in the gap between the ultramicroelectrode (UME) tip and the substrate. In this configuration, the device is particularly attractive for measuring fast reaction rates, because at small tip-substrate separations, high rates of diffusion are attainable in the feedback mode.^{10,11}

An advantage of the SECM is that the response of the device can be calculated theoretically, with no adjustable parameters, by solving the appropriate diffusion equations with the electrochemical boundary conditions describing the situation of interest. Previous theoretical treatments have dealt with the steady-state⁴ and the chronoamperometric¹² feedback response for conducting and insulating substrates, positive (diffusion-controlled) and negative feedback, respectively, and the case where the tip-generated mediator decomposes homogeneously in solution.¹¹ These theoretical models assume uniform reactivity over an infinite substrate, which is generally the case in kinetic studies^{10,11} but is an unrealistic situation with regard to imaging real heterogeneous substrates. Additionally, the SECM feedback mode with finite kinetics at an infinite substrate has not yet been addressed theoretically.

Given the recent practical developments in SECM in reaction-rate imaging⁶ and in the measurement of heterogeneous kinetics in general,¹⁰ the aim of this paper is to develop theoretical models for the SECM feedback mode with (i) finite heterogeneous electron-transfer (et) kinetics at the substrate and (ii) an arbitrary substrate size. These objectives are addressed using two independent approaches, which have previously proved appropriate

for treating SECM problems: (i) the alternating direction implicit (ADI) finite difference method^{11,13} and (ii) the analytical formulation of multidimensional integral equations (MIE) and their numerical solution.^{14,15} The theoretical results are compared with feedback experiments for both irreversible and quasi-reversible kinetics at the substrate and with model finite substrates.

Theory

Finite Heterogeneous Kinetics at the Substrate. A schematic model defining the SECM feedback mode with finite kinetics at the substrate is given in Figure 1. The tip electrode is held at a potential at which the electrolysis of the target solution species (reduction of O to R in the example) is diffusion-limited. Earlier theoretical treatments of the SECM^{4,11,12} have considered only the cases where the tip-generated species, R, was either unreactive at the substrate (i.e., $k_{b,s} \rightarrow 0$ at an insulator) or reacted at a rate much larger than the rate of diffusion of R to the substrate (i.e., $k_{b,s} \rightarrow \infty$ at a "conductor"). We now consider the case where O is regenerated from R at a substrate of infinite size at a finite rate and diffuses back to the tip electrode, thereby establishing the feedback condition. An experimental study involving this situation has previously appeared.¹⁰ The rate constants for oxidation (k_b) and reduction (k_f) at the tip and substrate are given by the Butler-Volmer relations:¹⁶

$$k_f = k^0 \exp[-\alpha nF(E - E^0)/RT] \quad (1)$$

$$k_b = k^0 \exp[(1 - \alpha)nF(E - E^0)/RT] \quad (2)$$

(1) Bard, A. J.; Fan, F.-R. F.; Kwak, J.; Lev, O. *Anal. Chem.* **1989**, *61*, 132.

(2) Bard, A. J.; Denault, G.; Lee, C.; Mandler, D.; Wipf, D. O. *Acc. Chem. Res.* **1990**, *23*, 357.

(3) Bard, A. J.; Fan, F.-R. F.; Pierce, D. T.; Unwin, P. R.; Wipf, D. O.; Zhou, F. *Science* **1991**, *254*, 68.

(4) Kwak, J.; Bard, A. J. *Anal. Chem.* **1989**, *61*, 1221.

(5) Kwak, J.; Bard, A. J. *Anal. Chem.* **1989**, *61*, 1794.

(6) Wipf, D. O.; Bard, A. J. *J. Electrochem. Soc.* **1991**, *138*, L4.

(7) Lee, C.; Bard, A. J. *Anal. Chem.* **1990**, *62*, 1906.

(8) Lee, C.; Miller, C. J.; Bard, A. J. *Anal. Chem.* **1991**, *63*, 78.

(9) Lee, C.; Wipf, D. O.; Bard, A. J.; Bartels, K.; Bovick, A. *Anal. Chem.* **1991**, *63*, 2442.

(10) Wipf, D. O.; Bard, A. J. *J. Electrochem. Soc.* **1991**, *138*, 496.

(11) Unwin, P. R.; Bard, A. J. *J. Phys. Chem.* **1991**, *95*, 7814.

(12) Bard, A. J.; Denault, G.; Friesner, R. A.; Dornblaser, B. C.; Tuckerman, L. S. *Anal. Chem.* **1991**, *63*, 1282.

(13) Peaceman, D. W.; Rachford, H. H. *J. Soc. Ind. Appl. Math.* **1955**, *3*, 28.

(14) Mirkin, M. V.; Bard, A. J. *J. Electroanal. Chem. Interfacial Electrochem.*, in press.

(15) Mirkin, M. V.; Bard, A. J. *J. Electroanal. Chem. Interfacial Electrochem.*, in press.

[†] Present address: Department of Chemistry, University of Warwick, Coventry CV4 7AL, U.K.

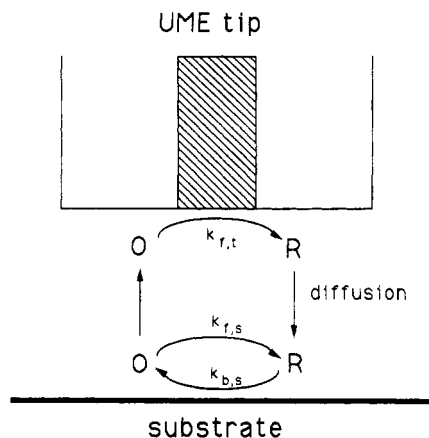


Figure 1. Schematic illustration of the SECM feedback mode with finite heterogeneous kinetics. The magnitude of the rate constant for the tip electrode reaction, $k_{f,t}$, is such that the reaction $O \rightarrow R$ occurs at a diffusion-controlled rate.

where k° is the standard rate constant, E is the electrode potential, E° is the formal potential, α is the transfer coefficient, n is the number of electrons transferred per redox event, F is the Faraday constant, R the gas constant, and T is the temperature. The subscripts s and t will refer to the substrate and tip processes, respectively. Although the experiments reported in this paper relate to the case where the substrate is an electrode, the theoretical treatment developed here applies to any substrate regeneration reaction (e.g., surface-bound enzyme catalyzed redox processes).¹⁷

Two kinetic regimes are of particular interest and will be considered here: (i) quasi-reversible regeneration of O (both forward and back-reactions occur at the substrate at the applied potential, but the rates are insufficient, on the time scale of the experiment, for equilibrium to be attained) and (ii) irreversible regeneration of O at the substrate ($k_{f,s} \rightarrow 0$, $k_{b,s} \gg k_{f,s}$). The former case was treated using the MIE method,^{14,15} and the latter using the ADI method.^{11,13} Test calculations, reported below, indicated an excellent level of agreement between the two approaches. For both kinetic cases, the theoretical treatments considered the general transient (chronoamperometric) feedback response, but particular emphasis is placed here on the steady-state behavior (developed at long times).

The relevant time-dependent SECM diffusion equations for species R and O in dimensionless form are^{4,11,14}

$$\frac{\partial C_i}{\partial T} = \frac{\partial^2 C_i}{\partial Z^2} + \frac{\partial^2 C_i}{\partial R^2} + \frac{1}{R} \frac{\partial C_i}{\partial R} \quad 0 < T, 0 \leq R, 0 < Z < L \quad (3)$$

where L is the normalized tip-substrate distance (d/a), and the dimensionless variables are defined by

$$R = r/a \quad (4)$$

$$Z = z/a \quad (5)$$

$$C_i = c_i/c_O^\circ \quad (6)$$

$$T = tD_i/a^2 \quad (7)$$

where r and z are respectively the coordinates in the directions radial and normal to the electrode surface, D_i and c_i are the diffusion coefficient and concentration of the species i ($i = O, R$), c_O° is the bulk concentration of O , a is the tip electrode radius, and t is time.

In this paper, as previously,^{4,11,15} we consider the situation where $D_O = D_R = D$ with only the tip reactant (O in this case) initially present in solution. The first assumption allows the principle of mass conservation to be invoked:

$$C_R(R,Z) = 1 - C_O(R,Z)$$

and the problem can then be described in terms of a single species (O). The boundary conditions for the problem under these conditions are of the form

$$0 < T, 0 \leq R < 1, Z = 0 \quad (\text{tip electrode surface}); \\ C_O = 0 \quad (\text{ADI simulation}) \quad (8a)$$

or

$$\frac{\partial C_O}{\partial Z} = K_{f,t}C_O - K_{b,t}(1 - C_O); \quad K_{f,t} \gg K_{b,t} \\ (\text{integral equation method}) \quad (8b)$$

$$0 < T, 1 \leq R \leq RG, Z = 0 \\ (\text{glass insulating sheath}); \quad \frac{\partial C_O}{\partial Z} = 0 \quad (9)$$

$$0 < T, 0 \leq R \leq h, Z = L \quad (\text{substrate surface}); \quad \frac{\partial C_O}{\partial Z} = \\ K_{f,s}C_O - K_{b,s}(1 - C_O) \quad (10)$$

$$R = 0, 0 < Z < L \quad (\text{axis of symmetry}); \quad \frac{\partial C_O}{\partial R} = 0 \\ (\text{ADI simulation}) \quad (11)$$

$$R > RG, 0 \leq Z \leq L; C_O = 1 \quad (12)$$

where

$$K_{f/b,s} = k_{f/b,s}a/D; \quad K_{f/b,t} = k_{f/b,t}a/D \quad (13)$$

$$RG = r_g/a \quad (14)$$

$$h = a_s/a \quad (15)$$

where r_g is the radius of the tip insulating material and a_s is the active substrate radius. The initial condition, completing the definition of the problem, is

$$T = 0, 0 \leq R, 0 \leq Z \leq L; C_O = 1 \quad (16)$$

(i) Quasi-Reversible Kinetics. Preliminary results for this situation, where the tip radius and substrate are equal in size, were considered elsewhere¹⁵ using the MIE method. The results given here relate to the case where the substrate is infinite, (i.e., $h \rightarrow \infty$), which is the usual situation in kinetic studies.^{10,11} The necessary modifications to the computational algorithm are outlined in Appendix A.

For the quasi-reversible case, the UME feedback current depends on the magnitude of both the forward and back normalized rate constants and the SECM geometry (d/a). It is difficult to provide a complete set of working curves that will cover all experimental possibilities. We therefore provide results that illustrate the essential features of the feedback response in the quasi-reversible regime. Computational results for a range of kinetic situations, given in Table I, supply values of the dimensionless steady-state SECM current, $I_t = i_t/i_{t,\infty}$, where

$$i_{t,\infty} = 4nFDc_O^\circ a \quad (17)$$

is the steady-state current at a microelectrode at infinite separation from the substrate.^{18,19} Each I_t value was obtained as a limiting value of the transient current as $t \rightarrow \infty$. Each row in Table I corresponds to a given value of the normalized tip/substrate distance, L . Seven groups of columns (three columns in each group) correspond to various values of the dimensionless kinetic parameter $\Lambda (=ak^\circ_s/D)$, with Λ spanning the range of quasi-reversibility from virtually reversible ($\Lambda = 25$) to essentially irreversible processes ($\Lambda = 0.001$). Three contrasting values of the dimensionless substrate potential, $E_1 = (E_s - E^\circ)nF/RT$, were considered for each Λ ; these correspond to the formal potential, a potential where the substrate feedback reaction is almost diffusion-controlled, and a potential between the two. An α value of 0.5 was assumed for all calculations.

(16) Bard, A. J.; Faulkner, L. R. *Electrochemical Methods*; Wiley: New York, 1980; pp 95-110.

(17) Pierce, D. T.; Bard, A. J. Unpublished results.

(18) Saito, Y. *Rev. Polarogr.* **1968**, *15*, 177.

(19) Wightman, R. M.; Wipf, D. O. In *Electroanalytical Chemistry*; Bard, A. J., Ed.; Marcel Dekker: New York, 1988; Vol. 15, p 267.

TABLE I: SECM of Normalized Steady-State Current Computed for Various Values of the Kinetic Parameter, Λ , Normalized Tip-Substrate Distance, L , and Dimensionless Substrate Potential, E_1^a

| L | $\Lambda = 25$ | | | $\Lambda = 5$ | | | $\Lambda = 1$ | | | $\Lambda = 0.5$ | | $\Lambda = 0.1$ | | | $\Lambda = 0.05$ | | | $\Lambda = 0.001$ | | | |
|-----|----------------|-------|-------|---------------|-------|-------|---------------|-------|-------|-----------------|-------|-----------------|------|-------|------------------|------|-------|-------------------|------|-------|------|
| | E_1 | | | E_1 | | | E_1 | | | E_1 | | E_1 | | | E_1 | | | E_1 | | | |
| | 0.0 | 0.585 | 2.926 | 0.0 | 1.171 | 4.682 | 0.0 | 2.341 | 7.803 | 0.0 | 3.902 | 9.754 | 0.0 | 7.803 | 11.71 | 0.0 | 7.803 | 13.66 | 0.0 | 15.61 | 21.4 |
| 0.1 | 3.71 | 4.79 | 7.66 | 2.40 | 3.84 | 7.38 | 1.00 | 2.42 | 7.39 | 0.68 | 2.62 | 7.67 | 0.21 | 3.25 | 6.95 | 0.17 | 2.07 | 7.31 | 0.11 | 2.04 | 7.30 |
| 0.2 | 2.12 | 2.74 | 4.20 | 1.66 | 2.62 | 4.22 | 0.93 | 2.05 | 4.24 | 0.72 | 2.22 | 4.32 | 0.24 | 2.59 | 4.10 | 0.19 | 1.89 | 4.22 | 0.14 | 1.86 | 4.21 |
| 0.5 | 1.16 | 1.48 | 2.20 | 1.07 | 1.62 | 2.26 | 0.84 | 1.61 | 2.28 | 0.69 | 1.72 | 2.29 | 0.49 | 1.87 | 2.25 | 0.43 | 1.60 | 2.27 | 0.36 | 1.60 | 2.27 |
| 0.8 | 0.89 | 1.14 | 1.68 | 0.85 | 1.30 | 1.74 | 0.78 | 1.39 | 1.76 | 0.68 | 1.49 | 1.76 | 0.60 | 1.58 | 1.75 | 0.57 | 1.44 | 1.76 | 0.50 | 1.44 | 1.76 |
| 1.0 | 0.81 | 1.03 | 1.51 | 0.79 | 1.18 | 1.57 | 0.72 | 1.31 | 1.58 | 0.67 | 1.40 | 1.58 | 0.61 | 1.47 | 1.57 | 0.60 | 1.37 | 1.58 | 0.55 | 1.37 | 1.58 |
| 1.5 | 0.70 | 0.89 | 1.32 | 0.69 | 1.03 | 1.35 | 0.68 | 1.18 | 1.36 | 0.67 | 1.27 | 1.36 | 0.66 | 1.31 | 1.35 | 0.66 | 1.26 | 1.36 | 0.67 | 1.26 | 1.36 |
| 2.0 | 0.66 | 0.82 | 1.21 | 0.65 | 0.96 | 1.24 | 0.66 | 1.12 | 1.25 | 0.66 | 1.19 | 1.25 | 0.70 | 1.22 | 1.25 | 0.73 | 1.20 | 1.25 | 0.78 | 1.20 | 1.25 |
| 5.0 | 0.63 | 0.78 | 1.05 | 0.64 | 0.90 | 1.08 | 0.65 | 1.01 | 1.08 | 0.66 | 1.06 | 1.08 | 0.74 | 1.07 | 1.08 | 0.79 | 1.07 | 1.08 | 0.92 | 1.07 | 1.08 |

^a $L = d/a$, $E_1 = (E_s - E^{\circ})nF/RT$, $\Lambda = ak^{\circ}_s/D$, and $\alpha = 0.5$ for all cases.

Table I indicates that an increase in the overpotential (while keeping the values of the other parameters constant) leads to a higher feedback current. At sufficiently high overpotentials, the substrate behaves like a conductor with diffusion-controlled feedback, and the I_t vs L dependence is similar to that reported previously for this condition,⁴ i.e., with increasing L , I_t decreases monotonically to unity. At $E_1 = 0$ and small Λ , the rate of the feedback process at the substrate is negligible; the substrate behaves like an insulator, and the tip current increases with L . However at $E_1 = 0$ and large Λ , a significant positive feedback is observed with a small L . With the same E and Λ at longer distances, the current is even lower than in the case of the completely insulating substrate. In this situation, some reduction of O occurs at the substrate so that O is depleted in the gap and the flux of O to the tip is diminished. Here the substrate shields (in the ring-disk electrode sense) the tip.

The apparent reversibility of the electrochemical process increases with L (since the diffusion rate to the tip decreases with increasing tip-substrate distance), and the values of I_t for intermediate E_1 approach those for large E_1 . The I_t vs L characteristics can be used to determine Λ at the substrate electrode, for example, the diagnostic case of $\Lambda = 1.5$ and $E_1 = 0$, where the value of I_t is almost independent of L .

(ii) **Irreversible Kinetics.** This special case of the general kinetic problem outlined above (with $K_{f,s}$ set to zero) was treated with the ADI method to provide a completely different approach and a check on the computations. A general description of the application of this method to the treatment of SECM problems is given elsewhere.¹¹ Additional details relevant to the present study are provided in Appendix B. The ADI method yields the transient (chronoamperometric) response. It is useful to consider the chronoamperometric behavior, since this can provide complementary information to steady-state measurements, as illustrated in the study of homogeneous kinetics.¹¹

Typical transients (presented as normalized current vs $T^{-1/2}$)^{11,12} with various rate constants ($K_{b,s}$) for oxidation of R are shown in Figure 2. These data are for an SECM geometry characterized by $L = 0.1$, and $RG = 10$. The latter parameter was used in all ADI calculations. The corresponding behaviors for both a conducting and insulating substrate (i.e., $K_{b,s} \rightarrow \infty$ and $K_{b,s} \rightarrow 0$, respectively) are also shown for comparison. The forms of these limiting responses were described in detail earlier.¹² With finite kinetics at the substrate, the feedback characteristics depend upon the relative rates of diffusion and surface et. (The magnitude of the former quantity is governed, in part, by the time scale of the chronoamperometric measurements,^{11,12} with the lowest rates obtained under steady-state conditions for a particular tip-substrate separation.) The faster the rate of the substrate reaction (compared to the rate of diffusion), the higher the feedback current. In general, steady-state measurements are likely to provide the most accurate and convenient means of measuring heterogeneous rate constants with the SECM. However, since the current-time behavior in the slow kinetic regime ($K_{b,s} < 1$) is essentially identical to that predicted for an insulating substrate for a significant portion of the chronoamperometric window (in the short-time region), this behavior can, in itself, be used to find the tip-substrate separation,¹² and transients may be useful, in

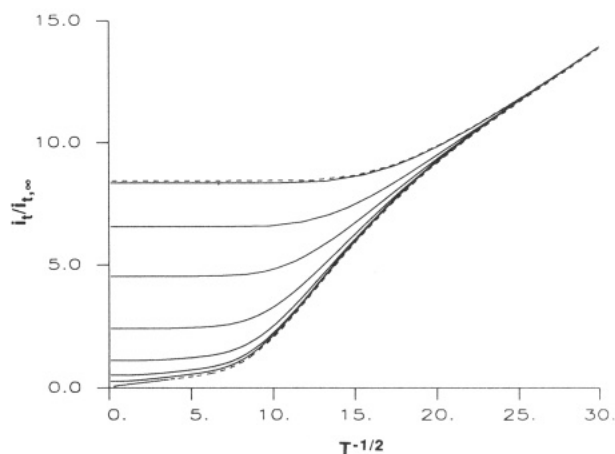


Figure 2. Simulated SECM feedback transients with various rate constants for the heterogeneous process at the substrate. The upper and lower dashed curves correspond respectively to the limits $K_{b,s} \rightarrow \infty$ and $K_{b,s} = 0$. The solid curves lying between these two extremes represent $\log K_{b,s} = 3.0$ (upper curve), 1.5, 1.0, 0.5, 0.0, -0.5, and -1.0 (lower curve). $RG = 10$.

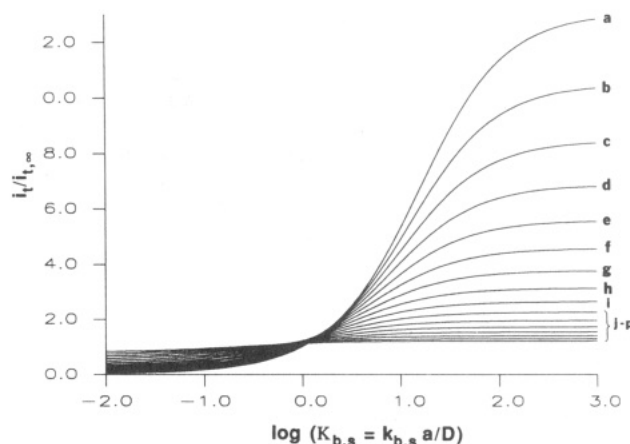


Figure 3. Working curves of I_t vs $\log K_{b,s}$ for $\log(d/a) = -1.2, -1.1, -1.0, \dots, 0.3$ (a-p).

addition to steady-state measurements, if an independent value of L is required.

Turning to the steady-state characteristics, theoretical working curves of normalized steady-state tip current vs $K_{b,s}$ for various tip-substrate separations are shown in Figure 3. These curves can be used to determine a rate constant for the substrate reaction. Experimentally, the largest rate constants are accessible and the accuracy is greatest when the tip-substrate distance is minimized.

The SECM approach appears particularly useful in the measurement of large k° values for electrode reactions. In general, in the measurement of a heterogeneous rate constant, the et step must be rate-determining, i.e., slower than mass transfer to the surface. Thus, ultramicroelectrodes are useful for such et rate constant measurements, since the rate of diffusion for disk or

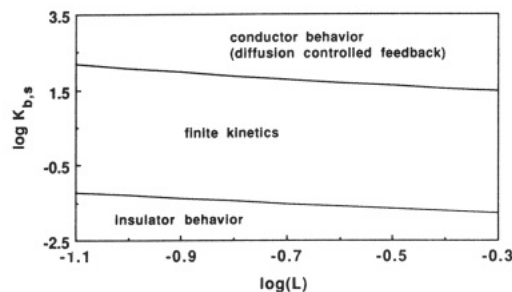


Figure 4. Kinetic zone diagram illustrating the regions of finite irreversible kinetics, diffusion-controlled feedback, and insulating substrate behavior.

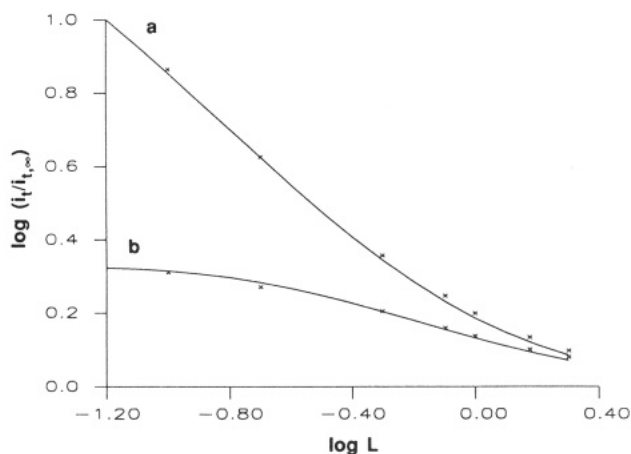


Figure 5. Comparison of the results of the MIE (×) and ADI (—) methods for (a) $K_{b,s} = 44.8$ ($K_{f,s} = 2.23 \times 10^{-8}$, MIE method) and (b) $K_{b,s} = 2.41$ ($K_{f,s} = 4.14 \times 10^{-7}$, MIE method).

spherical electrodes increases as the radius decreases.^{19,20} For example, for a disk of radius a , the steady-state mass-transfer constant, m ,²¹ is $4D/\pi a$. Thus, for $a = 1 \mu\text{m}$ and $D = 1 \times 10^{-5} \text{ cm}^2/\text{s}$, $m \approx 0.1 \text{ cm/s}$, which determines the upper accessible k° from steady-state measurements. However, in SECM measurements the mass-transfer constant is effectively D/d at close tip-substrate distances, so that the steady-state limit for measuring k° is governed by the tip-substrate spacing. A more accurate representation of the range of measurable rate constants from the calculations is readily identified by analyzing the steady-state characteristics in terms of a kinetic zone diagram. A plot for the values of L over which kinetic determinations are most accurate is shown in Figure 4. In deriving this figure, finite kinetics were assumed to operate in the zone defined by

$$0.9[i_{t,L}(\text{in}) - i_{t,\infty}] < [i_{t,L} - i_{t,\infty}] < 0.9[i_{t,L}(\text{con}) - i_{t,\infty}] \quad (18)$$

where $i_{t,L}$ denotes the tip current at a normalized tip-substrate distance, L , and the terms con and in refer to the limits for (diffusion-controlled) conductive and insulating feedback. In eq 18, the upper and lower bounds correspond respectively to essentially conducting or insulating substrate behavior, given typical experimental accuracy. It follows from Figure 4 that if close tip-substrate distances can be achieved (e.g., $\log L = -1.1$), it should be possible to resolve normalized rate constants as large as 200. With typical SECM tip radii of 1–12.5 μm ^{1,8,10,11} and a value for D of $10^{-5} \text{ cm}^2 \text{ s}^{-1}$, rate constants in the range 1.6–20 cm s^{-1} should be accessible to measurement (in the fast kinetic domain).

Comparison of the MIE and ADI Methods. A check of the computations can be accomplished by a comparison of the steady-state behaviors calculated with the MIE method (for kinetic cases where the quasi-reversible regime approaches irreversibility)

(20) Fleischmann, M.; Pons, S.; Schmidt, P. P. *Ultramicroelectrodes*; Datatech Systems, Inc.: Morgantown, NC, 1987.

(21) Bard, A. J.; Faulkner, L. R. *Electrochemical Methods*; Wiley: New York, 1980; p 28.

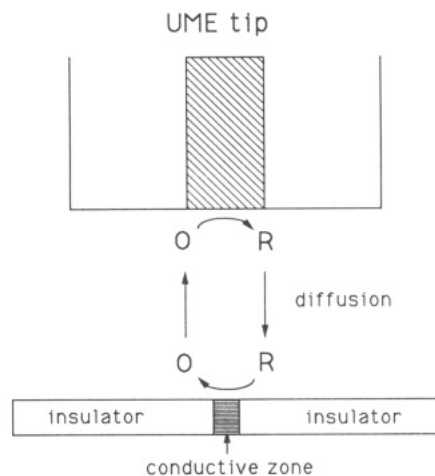


Figure 6. Schematic illustration of the SECM feedback mode with a finite substrate. The heterogeneous redox reactions occur at a diffusion-controlled rate at the UME and conductive portion of the substrate.

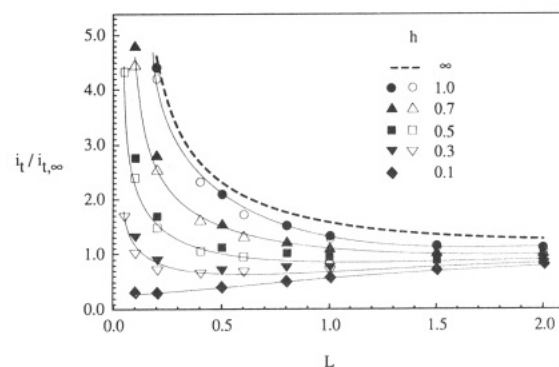


Figure 7. Simulated I_t vs L curves for finite disk-shaped substrates: (filled symbols) MIE simulation; (open symbols) ADI simulation. The h values are as indicated: (—) simulation for h^∞ from ref 4. The lines through the symbols are drawn as a guide. $RG = 10$.

and the ADI method (Figure 5). The level of agreement between the two independent approaches serves to validate the theoretical results presented above.

SECM with an Arbitrary Substrate Size. Most theoretical treatments of the SECM experiment assume a substrate feature size that is much larger than the tip diameter (i.e., an infinite substrate).^{4,11,12} However, in imaging with the SECM, questions of resolution of surface features (e.g., a conductive spot on an insulating plane) arise. What is the range of size of features resolvable with the SECM? In particular, what is the smallest feature that can be resolved? At what size does a finite-sized substrate behave like an infinite one?

A schematic model representing SECM in the feedback mode with a finite substrate is shown in Figure 6. The tip electrode reaction is as defined above, but now only a portion of the substrate is reactive in terms of the regeneration of O from R, which is assumed to occur at a diffusion-controlled rate. For simplicity, we consider this portion of the substrate to be circular (radius a_s in r space and h (eq 15) in normalized radial space) and centered at $R = 0$. The species R and O are assumed to be inert on the substrate surrounding this area. The boundary conditions, eqs 8, 9, and 11, again apply to this SECM problem.

Working curves, for various substrate sizes, representing the dependence of the steady-state diffusion-controlled current on the dimensionless distance between the tip and the substrate are shown in Figure 7. These were computed independently using both the MIE and ADI methods; the level of coincidence of the data obtained via the two techniques assures the reliability of the computational results.

As expected, the larger the value of h , the closer is the current-distance behavior to that for an infinite conductive substrate⁴ (represented by the dashed line in Figure 7); while for smaller

h , the behavior is closer to that for an insulating substrate.⁴ For substrates of intermediate size, the behavior is more complicated. When L is small, positive feedback ($i_t > i_{t,\infty}$) is observed, but at larger d , the substrate looks more like an insulator ($i_t < i_{t,\infty}$). The computed current–distance curves can be used to estimate the dimensionless substrate size, h^* , at which the substrate can be considered to be infinite; empirically

$$h^* = 1 + 1.5L \quad (19)$$

For example, if $L = 0.1$, a substrate with $h \geq 1.15$ behaves essentially as an infinite one, but if $L = 2$ the substrate looks infinite at $h \geq 4$. The value of h^* defines the surface area which is actually seen in an SECM feedback experiment and thus has important implications in terms of the resolution of SECM images. In particular, the highest resolution is obtained at close tip–substrate separations.

At small L , e.g., $L = 0.1$, there is a substantial difference between the steady-state feedback current for the insulating substrate and that for a finite substrate with $h = 0.1$. Since the lowest experimentally achievable L value is somewhat smaller than 0.1,^{10,22} it should be possible to identify particles (or other objects) 10–20 times smaller than the tip by SECM (if these particles are sufficiently well separated.) With a tip 1 μm in diameter, this corresponds to particles 50–100 nm in size.

Experimental Section

Reagents. $\text{Fe}_2(\text{SO}_4)_3$ (Puratronic, Alfa, West Hill, MA) and $\text{Ru}(\text{NH}_3)_6\text{Cl}_3$ (Strem Chemicals, Newburyport, MA) were used as received. Electrolyte solutions were 1 M sulfuric acid in deionized water (Milli-Q, Millipore) or phosphate–citrate (McIlvaine) buffers made to 0.5 M ionic strength with KCl.

Electrodes. Ultramicroelectrode tips were prepared from 10- μm -diameter platinum (Goodfellow Metals, Cambridge, U.K.) or 25- μm -diameter gold wire (Alfa) as described previously.¹⁰ The substrate electrode was a 3.0-mm-diameter glassy-carbon disk electrode (BAS, West Lafayette, IN). Microdisk substrates of different sizes were constructed by sealing 10-(Goodfellow), 25-, 100-, and 250- μm -diameter Pt (Alfa) wires in glass tubes. A number of these tubes were then potted in epoxy (EPON 828, Miller Stephenson, Danbury, CT), and the epoxy–glass composite was ground to expose the Pt microdisks. Both the substrate and tip electrodes were polished with 0.05- μm alumina on felt (Buehler, Ltd., Lake Bluff, IL) before each experimental run. No other electrode pretreatment was applied. All potentials were recorded vs a Hg/Hg₂SO₄ reference electrode in 1 M sulfuric acid (MSE) or a Ag/AgCl. The auxiliary electrode was Pt gauze or wire.

Apparatus. A four-electrode potentiostat (EI-400, Ensmann Instruments, Bloomington, IN), designed for low-current measurements, was used for independent control of the tip and substrate potentials. Other details of the SECM apparatus have been described.^{1,5,10}

SECM Procedure. For all of the SECM experiments, the tip current (i_t) and the tip position were recorded as the tip was scanned in a direction perpendicular to the substrate surface (z direction) at speeds of 0.2–0.5 $\mu\text{m s}^{-1}$. As in previous SECM studies, the tip current was not used as part of a closed-loop control system (as is done for the scanning tunneling microscope). Whenever possible, the current–distance curves were converted to absolute distance by fitting the experimental curves to a simulation for the diffusion-controlled steady-state current–distance curve. The distance scale was made dimensionless by dividing by the tip electrode radius (a). The experimental feedback current was normalized by dividing by the steady-state current obtained when the tip was far from the substrate ($i_{t,\infty}$).

Results and Discussion

Quasi-Reversible ET Kinetics at the Substrate. For the case of quasi-reversible kinetics at the substrate, both the forward and back electron-transfer (et) reactions must be considered. For example, the reduction of species O can be made to occur at a

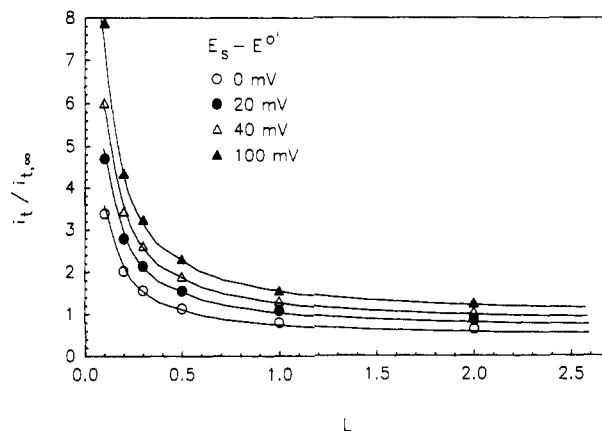


Figure 8. Experimental and simulated current–distance data for a quasi-reversible substrate process. The solid lines are experimental data for a 1.7 mM solution of $\text{Ru}(\text{NH}_3)_6^{3+}$ in a pH 4.0 buffer. The tip is a 12.5- μm -radius Au disk. The substrate is a GC electrode biased at potentials of 0, 20, 40, and 100 mV positive of the formal potential. The symbols are for a MIE simulation with $\Lambda = 15$ at the potentials indicated.

diffusion-controlled rate by application of a sufficiently negative tip potential. Species R diffuses to the substrate where the et rate of the forward (oxidation) reaction at the applied substrate potential controls the feedback effect. However, over a range of substrate potentials, a net back et reaction (i.e., reduction of O) can occur to deplete the bulk mediator concentration at the substrate surface and in the tip–substrate gap. This depletion of the mediator complicates the SECM analysis.

The effect of quasi-reversible kinetics on the experimental SECM response was modeled for a mediator solution of $\text{Ru}(\text{NH}_3)_6^{3+}$ in a pH 4.0 buffer at a glassy-carbon (GC) substrate. Previous reports of the voltammetry of $\text{Ru}(\text{NH}_3)_6^{3+}$ at GC electrodes have indicated that the standard rate constant, k^0 , is in the range 10^{-2} – 10^{-3} cm s^{-1} and depends on both electrode pretreatment and solution pH.^{23,24} The diffusion coefficient for $\text{Ru}(\text{NH}_3)_6^{3+}$ in the pH 4.0 buffer was 6.3×10^{-6} $\text{cm}^2 \text{s}^{-1}$, as measured by the limiting current at an ultramicroelectrode disk.¹⁹ Current–distance curves for the $\text{Ru}(\text{NH}_3)_6^{3+}$ mediator were acquired at a 12.5- μm radius gold tip electrode (Figure 8). The tip was biased at -0.13 V vs the $\text{Ru}(\text{NH}_3)_6^{3+/2+}$ formal potential so that the $\text{Ru}(\text{NH}_3)_6^{3+}$ was reduced at a diffusion-limited rate. For each current–distance curve, the substrate was biased at the desired potential prior to acquiring data for 120 s. This delay allowed the concentration profile near the electrode surface time to equilibrate. Independent experiments indicate that, after the initial equilibration time, the tip, held at a constant distance, measured a constant current, indicating essentially no further bulk concentration change due to the substrate potential.

After the experimental data was acquired, simulations based on the MIE method were used to determine the standard rate constant for the $\text{Ru}(\text{NH}_3)_6^{3+/2+}$ couple on the GC electrode. With the assumption of a transfer coefficient, α , of 0.5, a good fit to the experimental results was obtained for the dimensionless kinetic parameter, Λ , of 15 (Figure 8), leading to a value of 0.076 cm s^{-1} for k^0 . Cyclic voltammetry of the $\text{Ru}(\text{NH}_3)_6^{3+/2+}$ couple at the GC electrode was used to confirm the indicated value. Determination of k^0 based on the cyclic voltammetric cathodic and anodic peak separations²⁵ indicated a rate constant of 0.037 cm s^{-1} . However, the cyclic voltammetric value is probably low because a small amount of ohmic drop contributes to the measured peak potentials. Thus, the SECM results appear to match well with the simulation and independent experimental results.

Irreversible ET Kinetics at the Substrate. A good experimental test system for irreversible heterogeneous et involves Fe(III) as

(23) McCreery, R. L. In *Electroanalytical Chemistry*; Bard, A. J., Ed.; Marcel Dekker: New York, 1991; Vol. 17, p 221.

(24) Deakin, M. R.; Stuts, K. J.; Wightman, R. M. *J. Electroanal. Chem. Interfacial Electrochem.* **1985**, *182*, 113.

(25) Bard, A. J.; Faulkner, L. R. *Electrochemical Methods*; Wiley: New York, 1980; p 23.

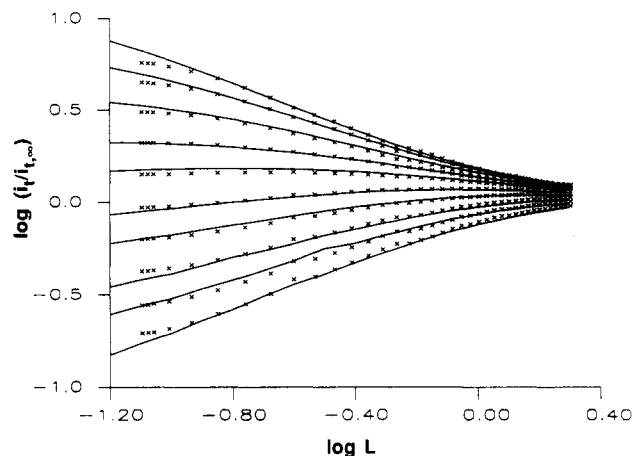


Figure 9. SECM log (current-distance) curves for the Fe(III)/Fe(II) system (X). The tip electrode (5.5- μm -radius carbon-fiber electrode) was held at a potential of -0.6 V , while the GC substrate electrode was held at various potentials, 300–750 mV, positive of the formal potential (50-mV increments). The corresponding best theoretical fits to the data, obtained with various values of $K_{b,s}$ (identified in Figure 10), are indicated by solid lines.

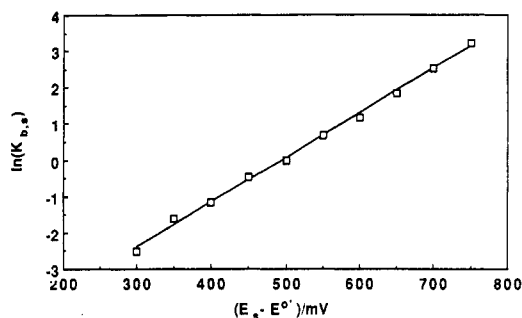


Figure 10. Plot of $K_{b,s}$ values deduced from the data in Figure 9 vs $(E_s - E^{\circ})$.

a mediator in 1 M sulfuric acid at a GC electrode. Previous work has shown that the standard rate constant for the Fe(III)/Fe(II) reduction at an unactivated GC electrode is about 10^{-5} – 10^{-6} cm s^{-1} .^{10,26} Because the standard rate constant is very small, the et process appears irreversible over a wide range of substrate potentials. In a previous paper, we examined the current-distance behavior for this system at various substrate potentials.¹⁰ For these experiments, the tip was an 11- μm -diameter carbon-fiber tip electrode held at -0.62 V (vs the Fe(III)/Fe(II) formal potential). At this potential, the tip generates Fe(II) at the diffusion-limited rate. The substrate was biased to various potentials where Fe(II) oxidation occurs, and current-distance curves were recorded (Figure 9). As shown, the tip feedback current decreased as the substrate potential was made less positive and the anodic et rate diminished. This experimental data was compared to simulations calculated with the ADI method. The simulation process involved simulating a large number of i_t - d curves for various values of the dimensionless, irreversible et rate constant, $K_{b,s}$. These curves were then matched to the experimental data to find the best fit of $K_{b,s}$ for each experimental i - d curve. The simulated $K_{b,s}$ values were used to obtain kinetic parameters for the electrode reaction. From eqs 2 and 13, it follows that

$$\ln K_{b,s} = \ln(k^{\circ}a/D) + (1 - \alpha)nF(E_s - E^{\circ})/RT \quad (20)$$

thus, a plot of $\ln K_{b,s}$ vs $(E_s - E^{\circ})$ will give α and k° . Figure 10 shows a plot of $\ln K_{b,s}$ vs the substrate potential. From linear regression, a slope of 12.3 V^{-1} and an intercept of -6.08 were calculated. Thus, α was found to be 0.69 and k° was $2.0 \times 10^{-5}\text{ cm s}^{-1}$ (with the assumption of an average D value of $4.8 \times 10^{-6}\text{ cm}^2\text{ s}^{-1}$ for Fe(II)/Fe(III)).²⁶ These kinetic parameters were used

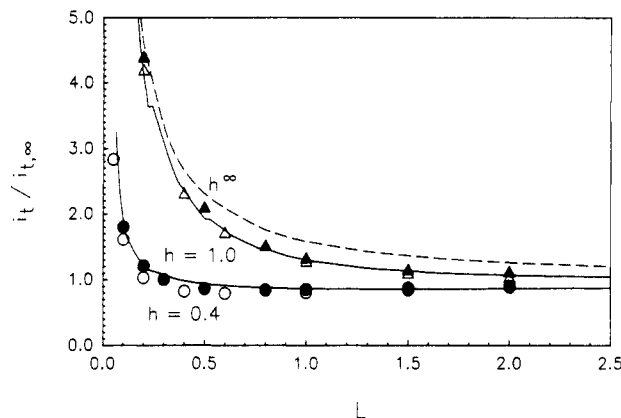


Figure 11. Experimental and simulated current-distance data at finite disk-shaped substrates. Solid lines are experimental curves acquired in a 2.4 mM solution of $\text{Ru}(\text{NH}_3)_6^{3+}$ in pH 4.0 buffer. The tip is a 12.5- μm -radius Au disk. The substrates are 5- and 12.5- μm -radius Pt disks. Symbols are simulations of finite-disk substrates for the MIE (filled symbols) and ADI (open symbols) methods.

to simulate the cyclic voltammetric wave for the Fe(III) mediator.²⁷ A good fit was found for the anodic wave, although the cathodic part of the cyclic voltammogram did not fit as well. Agreement with the anodic process is expected since the SECM data represent only these potentials.

Experimental Finite Substrate Effect. The effect of finite substrate size was examined experimentally by collecting current-distance curves over various sizes of microdisk substrates. The tips used had radii of 5 and 12.5 μm , and the substrate radii were 5, 12.5, and 125 μm , so that the substrate to tip ratios, h , were 0.4 to 10. The mediator solution was 2.4 mM $\text{Ru}(\text{NH}_3)_6^{3+}$ in pH 4.0 buffer. The tips and substrates were biased at -0.13 and 0.47 V , respectively, vs the $\text{Ru}(\text{NH}_3)_6^{3+/2+}$ formal potential, to ensure that diffusion-limited et occurred at both tip and substrate. Prior to acquiring a current-distance curve over a tip-substrate combination, the tip position was carefully adjusted to lie directly centered over the substrate. This was accomplished by scanning the tip laterally (x and y direction) across the substrate until the observed tip feedback current was at its maximum value.

Current-distance curves collected for h ratios of 2.5–10 were practically indistinguishable from the simulated current-distance curve for an infinite substrate. However, current-distance curves for h ratios of 0.4 and 1.0 show a significant deviation from the infinite-substrate curve (Figure 11). Simulations, using both the MIE and ADI methods, of the finite-substrate curves are shown overlaid on the experimental data in Figure 11. The close agreement between the experimental and simulated curves confirms the accuracy of the simulation models.

Conclusions

The theoretical and experimental behavior of the feedback current in the SECM has been examined for conditions of quasi-reversible and irreversible et at the substrate. The good agreement between both the MIE and ADI simulation techniques and experimental data suggests that the theoretical behavior for these cases are modeled well and complement the existing theory for reversible (conducting) substrates.⁴ The theoretical results presented here should allow use of the SECM for quantitative determination of rapid heterogeneous et rate constants at microscopic domains on sample surfaces. The theoretical data will also be useful in interpreting images made with reaction-rate imaging, in which the et activity of surface is mapped by the SECM.^{6,17}

The effect of finite substrate size has also been examined. The effect of finite substrate dimensions has previously been poorly understood with respect to the effect on the feedback current and ability to resolve small regions with the SECM. The agreement

(26) Taylor, R. J.; Humfray, A. A. *J. Electroanal. Chem. Interfacial Electrochem.* 1973, 42, 347.

(27) Bard, A. J.; Faulkner, L. R. *Electrochemical Methods*; Wiley: New York, 1980; p 689.

found between MIE and ADI simulations and experimental data for model disk-shaped substrates allows a better understanding of images of small irregular substrate features. Additional work in this area is needed to understand kinetic effects at finite substrate regions and also to determine the ability of the SECM to resolve individual active regions closely spaced to similar active regions.

Acknowledgment. The support of this research by the Robert A. Welch Foundation and the National Science Foundation (Grant CHE 8901450) is gratefully acknowledged. P.R.U. thanks SERC for support through the award of a NATO Fellowship. Part of the computing resources for this work were provided by The University of Texas System Center for High Performance Computing.

Appendix A

Numerical Solution of Two-Dimensional Integral Equations for SECM with Unequal Tip and Substrate Radii. The SECM diffusion problem leading to the two-dimensional integral equations was formulated and solved in ref 14, and the algorithm for the numerical solution of those equations was discussed in ref 15. The calculations performed in the present paper are based on the numerical solution of the same system:

$$\frac{f_i(T,R) \exp(\alpha_i n_i f[E_i(T) - E^{o'}]) / \Lambda_i + 1}{1 + \exp(n_i f[E_i(T) - E^{o'}])} = -\frac{1}{2L} \int_0^x u \, du \int_0^\tau \frac{\exp\left(-\frac{R^2 + u^2}{4(T-\tau)}\right)}{T-\tau} I_0\left(\frac{Ru}{2(T-\tau)}\right) \times \left[f_s(\tau, u) \theta_4\left(0 \left| \frac{i\pi(T-\tau)}{L^2} \right.\right) + f_i(\tau, u) \theta_3\left(0 \left| \frac{i\pi(T-\tau)}{L^2} \right.\right) \right] d\tau \quad (\text{A1a})$$

$$\frac{f_s(T,R) \exp(\alpha_s n_s f[E_s(T) - E^{o'}]) / \Lambda_s + 1}{1 + \exp(n_s f[E_s(T) - E^{o'}])} = -\frac{1}{2L} \int_0^x u \, du \int_0^\tau \frac{\exp\left(-\frac{R^2 + u^2}{4(T-\tau)}\right)}{T-\tau} I_0\left(\frac{Ru}{2(T-\tau)}\right) \times \left[f_s(\tau, u) \theta_3\left(0 \left| \frac{i\pi(T-\tau)}{L^2} \right.\right) + f_i(\tau, u) \theta_4\left(0 \left| \frac{i\pi(T-\tau)}{L^2} \right.\right) \right] d\tau \quad (\text{A1b})$$

where $f_i(T,R) = -[\partial C(T,R,Z)/\partial Z]_{Z=0}$ and $f_s(T,R) = [\partial C(T,R,Z)/\partial Z]_{Z=L}$ are dimensionless diffusion fluxes to the tip and substrate surfaces and $x = \max(1, h)$; see ref 15 for other parameters. The normalized tip and substrate currents are expressed by

$$I_t(T) = -\frac{\pi}{2} \int_0^1 f_i(T,R) R \, dR \quad \text{and} \quad I_s(T) = -\frac{\pi}{2} \int_0^h f_s(T,R) R \, dR \quad (\text{A2})$$

The only difference between the present calculations and those done previously arises from the value of h , which was constant and equal to unity in that work but now is changeable. This results in a small modification of the algorithm. As shown in ref 15, the numerical solution of eq A1 requires the evaluation of double integrals of the type

$$\int_{a_{j-1}}^{a_j} u \, du \int_{T_{k-1}}^{T_k} \frac{\exp\left(-\frac{R^2 + u^2}{4(T-\tau)}\right)}{T-\tau} \times I_0\left(\frac{Ru}{2(T-\tau)}\right) \theta_3\left(0 \left| \frac{i\pi(T-\tau)}{L^2} \right.\right) d\tau \quad (\text{A3})$$

that appear to be completely different depending on whether the

point R_j belongs to the integration subinterval (a_{j-1}, a_j) or not (in the first case the inner integral is divergent). In the case here, unlike that in ref 15, the spatial grids over the tip and the substrate surfaces are not identical, and the algorithm should recognize whether $R_j \in (a_{j-1}, a_j)$ or not. In the first case, the direct evaluation of the double integral A3 is necessary, otherwise the results can be computed faster by using the approximate formula (eq 11) from ref 15.

We used various modifications of the spatial and temporal grids to assure the accuracy of computational results. This is especially important for the simulation of SECM curves with low feedback current (small substrate, low rate of the electrode reaction at the substrate, large L), where a long time is required to achieve steady-state, causing significant computational problems. In this case, the proper choice of the time limit corresponding to the apparent steady-state (substantiated in ref 15) assures the compatibility of the computational results with that obtained for $RG = 10$.

Appendix B

Alternating Direction Implicit (ADI) Method Calculations. For the finite irreversible kinetics problem with an infinite substrate, the general features of the ADI method calculations were as previously described.¹¹ The radial coordinate in the diffusion equation (eq 3) was again initially transformed with exponential functions, prior to the simulations, in order to effect an efficient solution to the problem. The computational algorithm is based upon solving two sets of tridiagonal matrix equations, as given by eqs A10 and A11 in ref 11. One of the advantages of the ADI method is that the introduction of finite kinetics into the SECM problem only changes a few of the terms in the computational algorithm from those of either diffusion-controlled positive feedback or negative feedback.

For the present problem, the relevant expressions for the terms in eq A10 of ref 3 are identical to those given for species R in Table I of ref 11 except that

$$d_{j,NZ-1} \quad (0 \leq j \leq NE + NG - 2) = [1 - 2\lambda_Z + \lambda_Z/(1 + K_{b,s}\Delta Z)] C_{j,NZ-1} + \lambda_Z C_{j,NZ-2} + \lambda_Z K_{b,s}\Delta Z / (1 + K_{b,s}\Delta Z) \quad (\text{B1})$$

where the parameters in eq B1 can be understood by referring to ref 11.

The terms appropriate to eq A11 of ref 11 for the present problem are also as given for species R in Table II of ref 11 except

$$b^{**}_{NZ-1} \quad (0 \leq j \leq NE + NG - 1) = \frac{1 + 2\lambda_Z - \lambda_Z/(1 + K_{b,s}\Delta Z)}{1 + 2\lambda_Z - \lambda_Z/(1 + K_{b,s}\Delta Z)} \quad (\text{B2})$$

$$d^{*}_{NZ-1} \quad (j=0) = \{1 - 2\lambda\rho(0)\} C^{*}_{0,NZ-1} + 2\lambda\rho(0) C^{*}_{1,NZ-1} + \lambda_Z K_{b,s}\Delta Z / (1 + K_{b,s}\Delta Z) \quad (\text{B3})$$

$$d^{*}_{NZ-1} \quad (1 \leq j \leq NE + NG - 1) = \lambda\rho(j) \left\{ 1 - \frac{\Delta\rho}{2} \left[1 + \frac{\exp(-ml\Delta\rho)}{s + m - m \exp(-ml\Delta\rho)} \right] \right\} C^{*}_{j-1,NZ-1} + [1 - 2\lambda\rho(j)] C^{*}_{j,NZ-1} + \lambda\rho(j) \left\{ 1 + \frac{\Delta\rho}{2} \left[1 + \frac{\exp(-ml\Delta\rho)}{s + m - m \exp(-ml\Delta\rho)} \right] \right\} C^{*}_{j+1,NZ-1} \quad (\text{B4})$$

Calculations typically employed 100 points on the finite difference grid in the radial direction over the insulating portion of the tip (e.g., NG in ref 11), with 100 points over the electrode (NE) and 200 points in the Z direction (NZ).

For the calculation of the steady-state normalized current- $K_{b,s}$ working curves (presented in Figure 3), as opposed to the chronoamperometric characteristics per se, it becomes extremely inefficient to employ eq 16 as the initial condition for each value of $K_{b,s}$. For these calculations, eq 16 was therefore only used as the initial condition in the evaluation of the steady-state current for $\log K_{b,s} = 3$ (corresponding to essentially diffusion-controlled feedback for the range of tip-substrate distances considered, i.e., $-1.2 \leq \log L \leq 0.3$). The value of $\log K_{b,s}$ was then successively

decreased in intervals of 0.1 (to $\log K_{b,s} = -2.0$), and the new steady-state current was evaluated at each $K_{b,s}$, using the steady-state concentration profile evolved at the previous value of $K_{b,s}$ as the initial condition. With this computational procedure, it was possible to generate working curves comprising 51 points in under 20 CPU minutes on a VAX 6410 mainframe computer.

For simulations of the finite substrate problem, the radial coordinate in the diffusion equation (eq 3) was left untransformed over the region $R = 0$ to the larger of the edge of the substrate or electrode, i.e., to $R = h$ or a . Beyond this limit, the radial coordinate was transformed with an exponential function similar to that in eqn A2 in ref 11. These changes required some modifications of the computational algorithm, but these should be self-evident on the basis of our earlier work.¹¹ The number of

grid points employed in the Z direction for these calculations depended upon the normalized tip-substrate separation, varying from 100 ($\log L = -1.2$) to 200 ($\log L = 0.3$). In the radial direction, the density and distribution of grid points depended upon the magnitude of h . For $h \leq 0.4$, calculations employed 100 points over the substrate (and thus a total of $100/h$ points over the electrode). For $0.5 \leq h \leq 1$, 250 points were utilized over the electrode, and for larger values of h , between 150 and 250 points were employed. Beyond the edge of the electrode (or substrate), between 100 and 200 points were necessary to give the desired level of accuracy.

Registry No. Ru(NH₃)₆²⁺, 19052-44-9; Fe, 7439-89-6; Pt, 7440-06-4; carbon, 7440-44-0.

Energetics of Surface Reactions on (100) Diamond Plane

Daoyang Huang and Michael Frenklach*

Department of Materials Science and Engineering, Pennsylvania State University, University Park, Pennsylvania 16802 (Received: August 20, 1991)

The energetics of several possible diamond (100) surface growth reactions was investigated by a semiempirical quantum chemical method. These reactions included thermal and radical-driven dehydrogenation, hydrogen atom migration, and diamond growth by the addition of methyl, acetylene, carbon monoxide, and carbon atoms. Some of the major findings are as follows: the calculated potential energy barrier for H₂ elimination from a (100)-(1×1) diamond dihydride forming a (2×1) surface dimer is in good agreement with experiment; diamond growth by CH₃ addition on a dihydrogenated (100)-(1×1) surface encounters a large potential energy barrier, yet the barrier is lower for the addition of CH₃ to a triplet surface diradical or to a monohydride dimer surface radical; CO addition reactions have substantial potential energy barriers; the energetics for the addition of C atoms onto a diamond (100)-(1×1) surface is very favorable; and the growth of diamond by the addition of C₂H₂ on a (100) surface is feasible and should be the energetically preferred channel for the growth on surface ledges and kinks.

Introduction

Identification of elementary reaction mechanisms responsible for the growth of diamond in chemical vapor deposition (CVD) has received increasing attention.¹ In our previous studies,^{2,3} semiempirical quantum chemical calculations were used to screen possible diamond-growth reactions occurring on the (111) diamond surface. The focus of the present study is to undertake a similar analysis for most likely candidates for diamond growth on the (100) surface.

Semiempirical quantum chemical calculations were used by Verwoerd⁴ and Mehandru and Anderson⁵ to study several structural and energetic properties of diamond surfaces. Using MNDO calculations on a nine-atom cluster, Verwoerd⁴ investigated equilibrium structures of monohydride and dihydride phases and concluded that there is a large difference between the desorption energies of the two phases, in agreement with the experimentally observed difference in the thermal desorption temperatures.

Mehandru and Anderson⁵ employed atom superposition and electron delocalization molecular orbital and band methods. Using a six-layer-thick slab, they analyzed the structures and energetics for surface reconstruction of the ideal diamond (100) surface and the effect of hydrogen atom adsorption on the hydrogen-free and monohydrogenated reconstructed surfaces. With a smaller, three-layer-thick C₄₀H₄₀ cluster having 12 carbon atoms on the reacting surface, these authors investigated adsorption, bonding, and migration of CH₂, CH₃, and C₂H₂ to vacant sites on the monohydrogenated surface. Mehandru and Anderson found that CH₂ and CH₃ bond strongly to these sites, and that C₂H₂ can form two single bonds to adjacent H vacancies. They suggested however that such chemisorption of acetylene is not likely to be involved in diamond growth.

Unfortunately, neither of these studies calculated reaction transition states and associated potential energy barriers nor did they consider surface reactions involving nonvacant sites, both being critical issues in searching for possible mechanisms of diamond growth. The objective of the present work is to investigate theoretically the feasibility of several (100) surface reactions, those that have been suggested or are likely to contribute to the growth of diamond. These reactions include thermal and radical-driven dehydrogenation, hydrogen atom migration, and diamond growth by the addition of methyl radicals, acetylene and carbon monoxide molecules, and carbon atoms, the most frequently invoked growth species. To provide common grounds for comparison with our previous results, we employ the same computational method.

Method

The energies were obtained, as in the previous studies,^{2,3} using the MNDO all-valence electron parametrization of the NDDO

(1) For example: *Diamond and Diamond-Like Films*; Dismukes, J. P., Purdes, A. J., Spear, K. E., Meyerson, B. S., Ravi, K. V., Moustakas, T. D., Yoder, M., Eds.; The Electrochemical Society: Pennington, NJ, 1989; *Carbon* 1990, 26 (6). *J. Mater. Res.* 1990, 5 (1). *Proceedings of the Second International Symposium on Diamond Materials*; Purdes, A. J., Angus, J. C., Davis, R. F., Meyerson, B. M., Spear, K. E., Yoder, M., Eds.; The Electrochemical Society: Pennington, N.J., 1991. *Diamond and Diamond-Like Films and Coatings*; Angus, J. C., Clausing, R. E., Horton, L. L., Koidl, P., Eds.; Plenum: New York, in press.

(2) Huang, D.; Frenklach, M.; Maroncelli, M. *J. Phys. Chem.* 1988, 92, 6379.

(3) Huang, D.; Frenklach, M. *J. Phys. Chem.* 1991, 95, 3692.

(4) Verwoerd, W. S. *Surf. Sci.* 1981, 108, 153.

(5) Mehandru, S. P.; Anderson, A. B. *Surf. Sci.* 1991, 248, 369.